Acknowledgement — The authors wish to acknowledge Dr. M. Leschziner of the Sonderforschungsbereich 80, University of Karlsruhe, for discussing the problem.

REFERENCES

1. J. N. Cannon, W. B. Krantz, F. Kreith and D. Naot, A study of transpiration from porous flat plates simulating plant leaves, *Int. J. Heat Mass Transfer* **22**, 469–483 (1979).
2. J. O. Hinze, *Turbulence* p. 167. McGraw-Hill (1959).
3. C. C. Lin, *Statistical Theories of Turbulence* p. 34. Princeton University Press (1961).
4. J. N. Cannon, A model study of transpiration from broad leaves, Ph.D. Thesis, University of Colorado (1971).

Int. J. Heat Mass Transfer. Vol. 23, pp. 568–571
0017-9310/80/0401-0568 $02.00/0

INTERFEROMETRIC MEASUREMENT OF HEAT TRANSFER DURING MELTING FROM A VERTICAL SURFACE

P. D. VAN BUREN and R. VISKANTA
Heat Transfer Laboratory, School of Mechanical Engineering, Purdue University, West Lafayette, IN 47907, U.S.A.

(*Received* 3 *August* 1979)

NOMENCLATURE

c,	specific heat;
Fo,	Fourier number, $\alpha t/L^2$;
Δh_f,	latent heat of fusion;
L,	height of heat exchanger;
Nu,	local Nusselt number defined by equations (1) or (2);
Pr,	Prandtl number, ν/α;
Ra_x,	local Rayleigh number, $[g\beta\lvert T_w - T_f\rvert x^3/\nu^2](\nu/\alpha)$;
Ste,	Stefan number, $c(T_w - T_f)/\Delta h_f$;
T,	temperature;
t,	time;
α,	thermal diffusivity;
β,	thermal expansion coefficient;
ν,	kinematic viscosity.

Subscripts

f,	refers to fusion;
i,	refers to interface;
0,	refers to initial (uniform) conditions;
x,	refers to local;
w,	refers to wall.

INTRODUCTION

THE PRESENT study was conducted to obtain evidence on the detailed temperature distribution and local heat transfer coefficients at both the heated vertical surface and the solid–liquid interface during melting of an initially isothermal solid near its fusion temperature. The work was motivated by the need to gain understanding of heat transfer processes in latent heat-of-fusion thermal energy storage systems [1]. Cost effective and thermally efficient storage systems which take advantage of the latent heat-of-fusion of a phase-change material are prerequisite for economic utilization of alternate energy sources such as solar, waste heat recovery and load levelling.

Photographic observations of melting from a vertical cylindrical heat source [2] and a vertical isothermal wall [3] have indicated marked deviations in the shape of the melt region from the solid–liquid interface positions that would be predicted by a pure conduction model. More melting took place at the top than near the bottom of the heated vertical surfaces. The change of the melt shape with time provided conclusive evidence of the importance of natural convection in the melted region. However, temperature distributions in the melt and local heat-transfer coefficients have not been reported. The analysis of melting from a vertical cylindrical heat source, including the effects of natural convection induced by temperature differences in the melt, similarly indicates marked deviations in the shape of the melt region from that which would be predicted by a pure conduction model [4]. Natural convection was also found to play a very important role in the melting of material contained in a rectangular cavity [5].

Experiments described in this paper provide detailed information about the heat-transfer processes which occur when a solid is melted from a vertical surface in contact with the material. Knowledge of heat transfer at the interface, for example, is essential in predicting the motion of the phase-change boundary during melting. The interferograms recorded furnish evidence of the role of natural convection in the melt and yield qualitative information about the flow field in the liquid.

EXPERIMENTS

A Mach–Zehnder interferometer of typical rectangular design, having 7.3 cm dia optics, was used to measure the temperature distribution in the liquid. A 10 mW He–He laser produced a beam which was expanded by a system of lenses and served as a light source. The use of a laser eliminated the need for a compensation in the reference path of the interferometer.

The test cell used in the experiments consisted of two independent units – a Plexiglass container, with inside dimensions of 10.8 cm high, 8.51 cm wide and 5.07 cm deep, having optical quality glass windows to hold the test fluid and a separate flat plate heat exchanger which was installed in the test cell. Care was taken in the construction of the test cell to insure that the faces were parallel. The vertical flat surface heat exchanger was machined from a copper block by milling channels in one face and then soldering a thin copper plate over the channels. The width of the heat exchanger was such

that it fit snugly in the test cell. The completed heat exchanger through which a fluid from a constant temperature bath could be circulated was installed vertically near one of the test cell walls.

A number of copper–constantan thermocouples, calibrated against an NBS standard, were installed on the heat exchanger to determine the temperature uniformity of the surface. Two additional thermocouples were installed to measure the reference temperature of the fluid 'far' from the heat exchanger wall.

The interference fringe pattern was focussed on the film plane of a Nikon F2AS, 35 mm camera, by a 177.7 mm–f/1.9 television camera lens. This lens was corrected for spherical aberration and other image defects.

A paraffin, *n*-heptadecane (n-$C_{17}H_{36}$) was chosen as a test fluid in the experiments. This paraffin was selected because it has a fusion temperature near room temperature, which is conducive for reducing heat gains/losses from the ambient laboratory environment. The liquid phase is transparent and of sufficient quality for optical measurements. Also, the physical and transport properties of *n*-heptadecane are fairly well documented, which allows for correlation of the data in terms of dimensionless parameters.

The test cell was filled with *n*-heptadecane (99% pure), and the paraffin was solidified. Precautions were taken not to entrap any air as the liquid solidified. The initial temperature of the solid was maintained close to the fusion temperature and was typically less than 1 K lower than the fusion temperature. Therefore, the small subcooling ($T_f - T_0$) is not expected to have much effect on the melting front motion. Ethanol from a bath at a temperature above T_f was circulated through the heat exchanger.

After the desired conditions were established in the test cell, ethanol at a predetermined temperature above T_f was circulated through the heat exchanger. Because of effective heat transfer, the surface temperature of the plate rapidly reached its steady state value. Thermocouple readings were recorded and interference fringe patterns were photographed using Kodak Photomicrography Film SO-410 at predetermined time intervals.

The interferograms were enlarged to enable measurement of the interference fringe position using a vernier microscope. The temperature distribution in the liquid, the temperature gradient at the heater surface and at the solid–liquid interface and the heat-transfer coefficients were determined using the data reduction procedure described by Hauf and Grigull [6]. In the experiments discussed the temperature difference, $T_w - T_f$, had to be kept below 5°C. The index of refraction of *n*-heptadecane is rather sensitive to temperature and thus even a small temperature difference can produce fringe densities which are too large for accurate interpretation.

RESULTS AND DISCUSSION

The photographs of some typical interferograms recorded during melting of *n*-heptadecane are illustrated in Fig. 1. The air–liquid interface curves upward in the immediate vicinity of the heated surface due to surface tension because at the top the test material was not in contact with a solid boundary but with air. The interferograms clearly show the isotherms in the liquid from which the natural convection circulation can be deduced. Interferograms could not be recorded at early times because the melt layer was not sufficiently wide to permit passage of enough light for constructing interference fringe patterns. The photographs also reveal that there is significantly more melting near the top of the heated surface. The melt layer becomes more non-uniform in thickness as the heating progresses, compare Figs. 1(a) and (b).

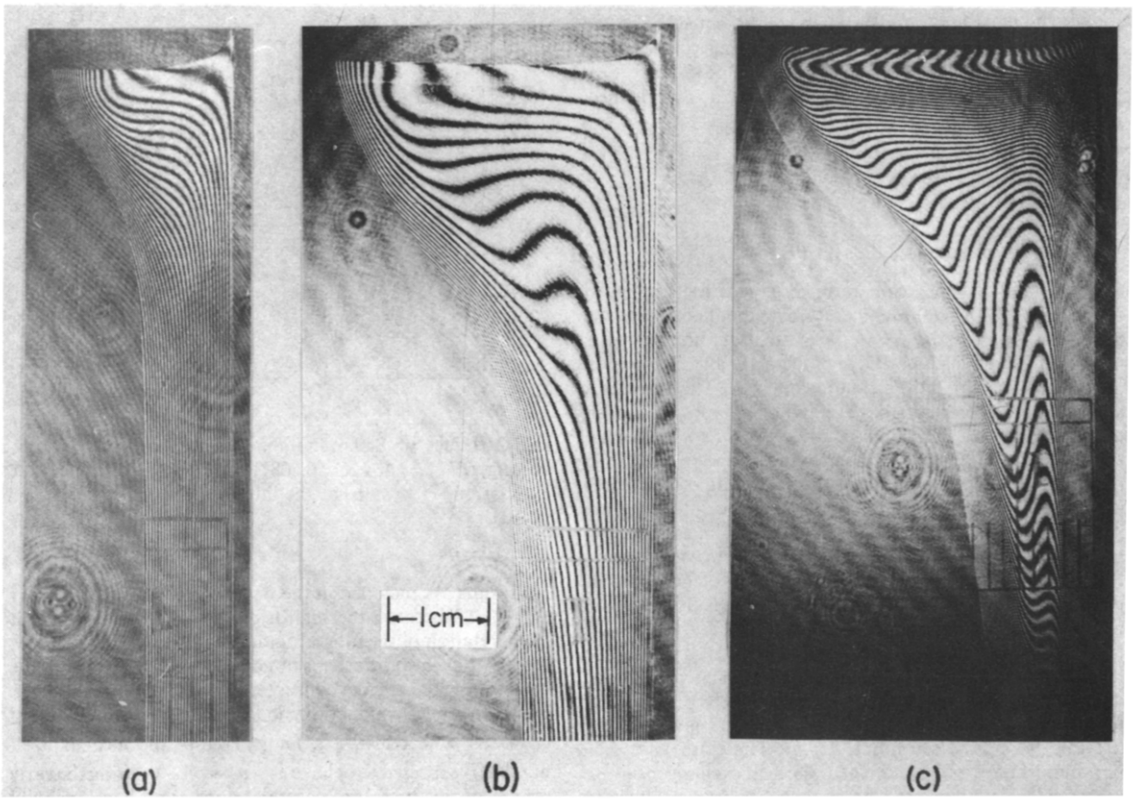

FIG. 1. Interferograms recorded during melting of *n*-heptadecane: (a) $Ste = 0.0128$ ($T_w = 22.5$°C), $Ra_L = 7.34 \times 10^6$ and $Fo = 0.355$, (b) $Ste = 0.0128$, $Ra_L = 7.34 \times 10^6$ and $Fo = 0.710$, (c) $Ste = 0.044$, $T_w = 25$°C, $Ra_L = 2.50 \times 10^7$ and $Fo = 0.202$.

The melt shapes are consistent with the presence of buoyancy induced, recirculating natural convection flow. The melt regions are similar to those observed recently [3]; however, less melting occurred at the top of the test cell in the experiments of [3] than those reported here. This is attributed primarily to the difference in the hydrodynamic conditions at the top. In the present experiments the surface of the material was free, e.g. exposed directly to air. This allowed expanded liquid to flow over the solid and promote melting near the top, while in the experiments of Hale and Viskanta [3] the material was completely enclosed, i.e. in contact with a solid wall at the top.

The local heat-transfer characteristics can be determined and the natural convection flow field can be inferred from the interferograms. The rather uniformly spaced interference fringes in the lower parts of Fig. 1(a) and (b) indicate that heat transfer is primarily by conduction in this region of the melt. As the fluid moves along the heated surface its temperature increases, and the temperature gradient decreases resulting in the minimum heat transfer rate at the top of the surface, see Fig. 1(b). The warm liquid is deflected towards the solid–liquid interface and melts the solid as it cools while descending along the phase-change boundary. The highest temperature gradients at the solid–liquid interface occur a small distance below the air–material interface. Flow reversal occurs some distance below this interface as evidenced by the interference fringe patterns. With continued heating, the melt volume increases in size, natural convection intensifies and a rather uniform temperature region develops in the upper part of the melt, see Fig. 1(b). For more intense heating (e.g. larger Stefan numbers) and/or later times distinct thermal boundary layers are formed, Fig. 1(c), at the heated surface and the interface. However, the high fringe density near the boundaries made it impossible to interpret the interferograms for the imposed thermal conditions.

The local heat-transfer characteristics along the heated surface and the solid–liquid interface are presented in Fig. 2 in terms of standard parameters for correlating transient natural convection in the absence of phase change [7]. The local Nusselt numbers at the surface and the interface are defined, respectively, as

$$Nu_x = -\partial T/\partial y|_w x/(T_w - T_f) \tag{1}$$

and

$$Nu_x = -\partial T/\partial n|_i x/(T_f - T_w) \tag{2}$$

where $\partial T/\partial y|_w$ is the temperature gradient at the heated surface and $\partial T/\partial n|_i$ is the temperature gradient normal to the phase-change boundary (interface). In equation (1) x is measured from the leading edge of the plate and in equation (2) it is measured from the air–liquid interface. The choice of x as a characteristic length scale may not be appropriate for transient natural convection heat transfer with solid–liquid phase change, because the volume and shape of the liquid region as well as the contour of the solid–liquid interface is changing continuously with time. Also, the interferogram illustrated in Fig. 1(c) suggests that either T_f in equation (1) or T_w in equation (2) may not be the appropriate reference temperatures for defining the heat transfer coefficients. The justification for defining Nu_x by equation (1) is that it would allow one to compare the results with those for steady and transient natural convection from a vertical plate in an infinite volume of fluid. It should also be emphasized that the nature of the Mach–Zehnder interferometer allows determination of only the average temperature gradient, e.g. $(\partial T/\partial y)_w$, along the width of the plate. Therefore, any small non-uniformities in the gradient at the heat exchanger surface are already accounted for. The local heat-transfer coefficients given by equations (1) and (2) should be considered as averaged values over the width of the test cell.

The effect of time on the dimensionless heat-transfer parameter $Nu_x/Ra_x^{1/4}$ at the plate surface is shown in Fig. 2(a).

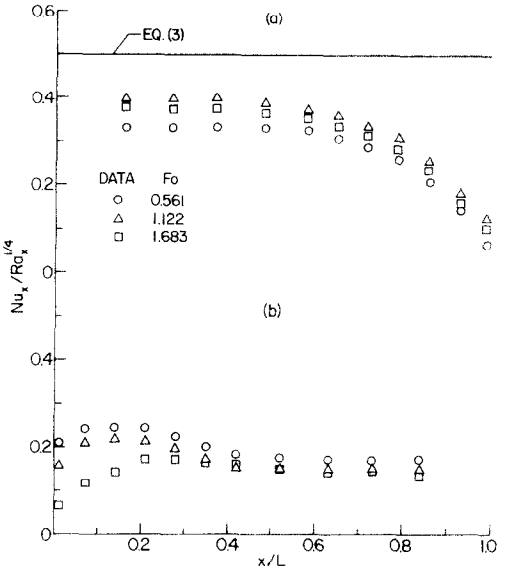

FIG. 2. Local heat transfer during melting, $T_w = 23°C$, $L = 3.49$ cm and $Ste = 0.0175$: (a) at the heated surface and (b) at the interface.

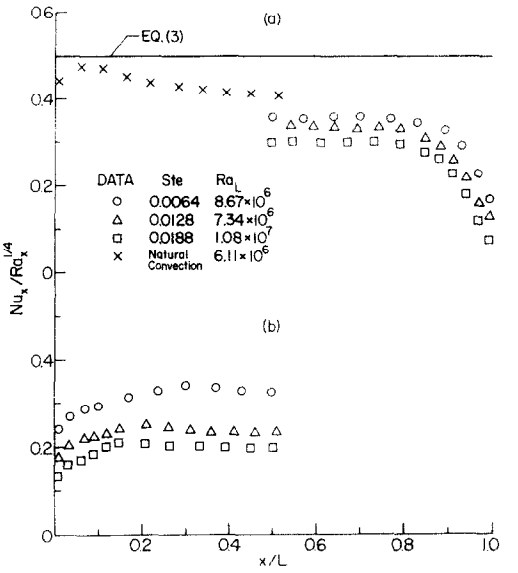

FIG. 3. Effect of Stefan number on heat transfer during melting, $L = 7.3$ cm, $Fo = 0.608$: (a) at the heated surface and (b) at the interface.

No results are included in the figure for $Fo < 0.561$ and for $x/L < 0.2$ because the high fringe density did not permit interpretation of the interferograms with sufficient accuracy. At early time heat transfer is by conduction, and the use of the heat-transfer coefficient concept may not be even meaningful. Based on a pure conduction model the melt layer thickness δ grows as $\delta = \text{const.}\sqrt{t}$, and therefore the local Nusselt number is expected to behave as $Nu_x \sim x/\sqrt{t}$ during the early stages of melting. As natural convection develops and intensifies the local Nusselt number approaches a maximum with time and then reverses. The reversal is attributable to the altered natural convection circulation flow as the size of the melt region increases and the shape changes with continued

heating. The net result of the competing processes is the decrease in the local heat-transfer coefficient with time. Steady state natural convection heat transfer from a vertical plate suspended in an infinite volume of liquid predicted by boundary-layer theory [8],

$$Nu_x/Ra_x^{1/4} = 0.503[1 + (0.492/Pr)^{9/6}]^{-4/9} \quad (3)$$

is included for the purpose of comparison. The predictions are seen to bound natural convection heat-transfer data in the presence of phase change and recirculation.

The largest heat-transfer coefficients along the solid–liquid interface occur near the top of the test cell where there is a 90° turn in the flow direction. The presentation of results in dimensionless form ($Nu_x/Ra_x^{1/4}$) also reveals this maximum. With continued heating and changing natural circulation flow in the melt region, the maximum moves down along the solid–liquid interface.

The effect of Stefan number on the heat-transfer coefficient at the heat surface and at the solid–liquid interface are presented in Figs. 3(a) and 3(b), respectively. Results could not be obtained for the lower part of the heated surface because the interferometer optics were too small to accommodate the entire cell. For comparison purposes, results are also included in Fig. 3(a) for transient natural convection heat transfer from a vertical surface in the absence of phase change. At this time (t = 45 min) quasi-steady natural convection appears to have been established, but because of thermal stratification in a finite-size test cell the heat-transfer parameter $Nu_x/Ra_x^{1/4}$ was not constant but decreased with the distance along the heated surface. At a given time, the heat-transfer coefficients at both the heated surface and the interface are seen to be lower for the higher Stefan numbers. This is attributed to a simultaneous occurrence of two main effects: (1) alteration of the natural convection flow field due to the change in size and shape of the melt region, and (2) modification of the temperature distribution. These changes are clearly seen in the interferograms presented in Fig. 1.

A meaningful comparison of the heat-transfer results ($Nu_x/Ra_x^{1/4}$) at the solid–liquid interface reported by Hale and Viskanta [3] with those of this work could not be made because of large differences in the Stefan and Rayleigh numbers as well as the hydrodynamic conditions at the top of the test cell. The results are in the range of those given in Fig. 3 (b).

The interferometer has provided detailed information about the heat transfer processes taking place at the heated surface and the interface which has not been reported in the literature previously, but the instrument is not without its limitations. The drawback of the interferometer is that at early times the melt layer is not sufficiently thick to permit the passage of enough light to produce sharp interference fringes. Consequently, temperature distribution data could not be obtained at early times when heat transfer by conduction predominated and/or natural convection was just beginning to develop because the melt layer was too thin. In addition, the index of refraction of n-heptadecane is very sensitive to temperature, and therefore only small superheats ($T_w - T_f$) could be used in the experiments to permit interpretation of the interferograms because of too large fringe density. The exploratory results reported in this note suggest that several additional effects and parameters must be considered in correlating natural convection heat transfer results during solid-to-liquid phase change in a finite-melt region.

Acknowledgements – This work was supported by the National Science Foundation Heat Transfer Program under Grant No. ENG-7811686.

REFERENCES

1. R. H. Turner, *High Temperature Energy Thermal Storage*. Franklin Institute Press, Philadelphia, 1978.
2. J. W. Ramsey and E. M. Sparrow, Melting and natural convection due to a vertical embedded heater, *J. Heat Transfer* **100C**, 368–370 (1978).
3. N. W. Hale, Jr. and R. Viskanta, Photographic observation of the solid–liquid interface motion during melting of a solid heat from an isothermal vertical wall, *Letters Heat Mass Transfer* **5**, 329–337 (1978).
4. E. M. Sparrow, S. V. Patankar and S. Ramadhyani, Analysis of melting in the presence of natural convection in the melt region, *J. Heat Transfer* **99C**, 520–526 (1977).
5. R. H. Marshall, Natural convection effects in rectangular enclosures containing a phase change material, in *Thermal Storage and Heat Transfer in Solar Energy Systems*, edited by F. Kreith *et al.* pp. 61–69. ASME, New York (1978).
6. W. Hauf and W. Grigull, Optical methods in heat transfer, in *Advances in Heat Transfer*, edited by T. F. Irvine, Jr. and J. P. Hartnett, Vol. 6, pp. 133–366. Academic Press, New York (1970).
7. J. D. Hellums and S. W. Churchill, Transient and steady state, free and natural convection numerical solutions—I. The isothermal, vertical plate, *A.I.Ch.E. Jl* **8**, 690–692 (1962).
8. S. W. Churchill and H. Ozoe, A correlation for laminar free convection from a vertical plate, *J. Heat Transfer* **95C**, 540–541 (1973).

Int. J. Heat Mass Transfer. Vol. 23, pp. 571–576

0017-9310/80/0401-0571 $02.00/0

MEASUREMENTS AND CALCULATIONS OF TRANSIENT NATURAL CONVECTION IN AIR

B. SAMMAKIA, B. GEBHART and Z. H. QURESHI
Department of Mechanical Engineering, State University of New York at Buffalo, Amherst, NY 14260, U.S.A.

(*Received* 16 *May* 1979 *and in revised form* 21 *August* 1979)

NOMENCLATURE

c_p, fluid specific heat;
c'', thermal capacity of element per unit surface area;
g, gravitational acceleration [m/s²];
G^*, $5\left[\frac{Gr_x^*}{5}\right]^{1/5}$;
Gr^*, non-dimensional modified Grashof number, $\frac{g\beta q'' x^4}{kv^2}$;
h, heat-transfer coefficient;
k, thermal conductivity [W/mK];
Pr, Prandtl number;